Intertropical Convergence Zone Variability in the Neotropics During the Common Era

Yemane Asmerom[1*], James U. L. Baldini[2], Keith M. Prufer[3], Victor J. Polyak[1], Harriet E. Ridley[2], Valorie V. Aquino[3], Lisa M. Baldini[4], Sebastian F. M. Breitenbach[5], Colin G. Macpherson[2] & Douglas J. Kennett[6]

[1]Department of Earth and Planetary Sciences, University of New Mexico, Albuquerque, New Mexico 87106, USA. [2]Department of Earth Sciences, University of Durham, Durham DH1 3LE, UK. [3]Department of Anthropology, University of New Mexico, Albuquerque, New Mexico 87106, USA. [4]Department of Geography, University of Durham, Durham DH1 3LE, UK. [5]Institute for Geology, Mineralogy & Geophysics, Ruhr-Universität Bochum, Universitätsstr. 150, 44801, Bochum, Germany [6]Department of Anthropology, The University of California, Santa Barbara, Santa Barbara, CA 93106, USA.
*Corresponding author, asmerom@unm.edu

Large changes in hydroclimate in the Neotropics implied by proxy evidence, such as during the Little Ice Age (LIA), have been attributed to meridional shifts of the Intertropical Convergence Zone (ITCZ), although alternative modes of ITCZ variability have also been suggested. Here we use seasonally-resolved stalagmite rainfall proxy data from the modern northern limit of the ITCZ in southern Belize, combined with records from across the Neotropics and subtropics, to fingerprint ITCZ variability during the Common Era. Our data are consistent with models that suggest ITCZ expansion and weakening during globally cold climate intervals, and contraction and intensification during global warmth. As a result, regions currently in the margins of the ITCZ in both hemispheres are likely transitioning to more arid and highly variable conditions, aggravating current trends of increased social unrest and mass migration.

INTRODUCTION

The Intertropical Convergence Zone (ITCZ) is the world's most important rainfall belt, affecting the livelihood of billions of people globally. Understanding its behavior during future warmer climate is thus vitally important. Intergovernmental Panel on Climate Change (IPCC) projections suggest that the Neotropics are particularly vulnerable to warming-induced droughts (*1*). On millennial timescales, shifts in ITCZ mean position likely reflect changes in the temperature contrast between the two hemispheres, with ITCZ migration towards the warmer hemisphere. However, the exact nature of the ITCZ response to global temperature changes remains unsettled. During the Common Era, substantial evidence now exists that climate change associated with the Little Ice Age (LIA) was global in extent (*2, 3*). Proxy records from the Neotropics suggest that the ITCZ shifted to the south during the LIA (*4-6*), however, recent model results (*7*) and limited observations elsewhere (*8, 9*) suggest that the ITCZ may have expanded in both hemispheres, while weakening in the central equatorial core region. Previous observations had several limitations, including combining monsoon and other proxies that are not necessarily reflective of purely ITCZ modulation (*5, 8*) or records not capturing the full ITCZ annual excursion (*4, 6*).

Figure 1. Locations of Yok Balum Cave (red circle) and other records discussed in the text. The average annual northernmost (July) and southernmost (January) margins are also shown (yellow and blue bands, respectively).

Here we use new monthly-scale speleothem rainfall proxy data from a cave site at the ITCZ's current northern margin in Central America coupled with published data from the southern margin of the ITCZ to explore its variability throughout the Common Era. We then use this information to determine whether the combined data are best explained by i) meridional ITCZ shifts exclusively or by ii) expansion and contraction of the ITCZ. The results have profound implications for predicting future hydroclimate of the global tropics.

Southern Belize, at the northern edge of the mean annual latitudinal range of the ITCZ (Fig. 1), is extremely sensitive to small variations in ITCZ position over time. The region receives between 400-700 mm of rainfall per month during the wet season (June to September) and ~10 times less during dry season months (February to April) due to seasonal ITCZ repositioning (*10*). Speleothem YOK-G was obtained from Yok Balum Cave in southern Belize (16° 12' 30.780" N, 89° 4' 24.420" W; Fig. S1). The cave has a stable temperature of 22.74 ± 0.09 °C (1σ) with high relative humidity approaching 100% throughout the year (Fig. S2).

RESULTS AND DISCUSSION

Stalagmite YOK-G is a very clean aragonitic speleothem with high uranium (U) and low detrital thorium (Th) concentrations that grew from 400 CE to 2006 CE (the year when it was collected). We measured 52 U-series ages (Table S1) using minimal amounts of powder to reduce errors related to drill-hole sizes and were able to obtain mean age uncertainties of seven years (2σ) across the entire record (Figure 2A). Details of our chronology and age model construction are discussed in the Materials and Methods section. Two previous studies (*11, 12*) reported on the upper portion of YOK-G (since 1550 CE). Here we present new YOK-G $\delta^{13}C$ and trace element datasets that extend the previously published YOK-G $\delta^{13}C$ record by 1,150 years. The complete YOK-G isotope record now consists of 7,151 $\delta^{13}C$ data points at ~0.22-year mean resolution overall, with monthly resolution across key intervals. The application of $\delta^{13}C$ as a rainfall proxy in YOK-G was previously established (*11-13*) . Additionally, here we use U

concentrations to confirm $\delta^{13}C$ as a rainfall proxy. Because U's partition coefficient in speleothem aragonite is very high (3.74 ± 1.13) (*13*), the amount of prior aragonite precipitation occurring above stalagmite YOK-G largely modulates U concentrations in the stalagmite. The excellent match between $\delta^{13}C$ and U concentrations across the study interval (r= -0.74, $p < 0.001$) (Fig. 2B) demonstrates that both proxies robustly reflect hydrologic variability despite their different exogenic cycles. While the correlation between $\delta^{18}O$ and U concentrations is not as strong (r=-0.44 , p <0.001) (Fig. S6) as that between $\delta^{13}C$ and U concentration, the $\delta^{18}O$ do capture the long-term changes in hydroclimate.

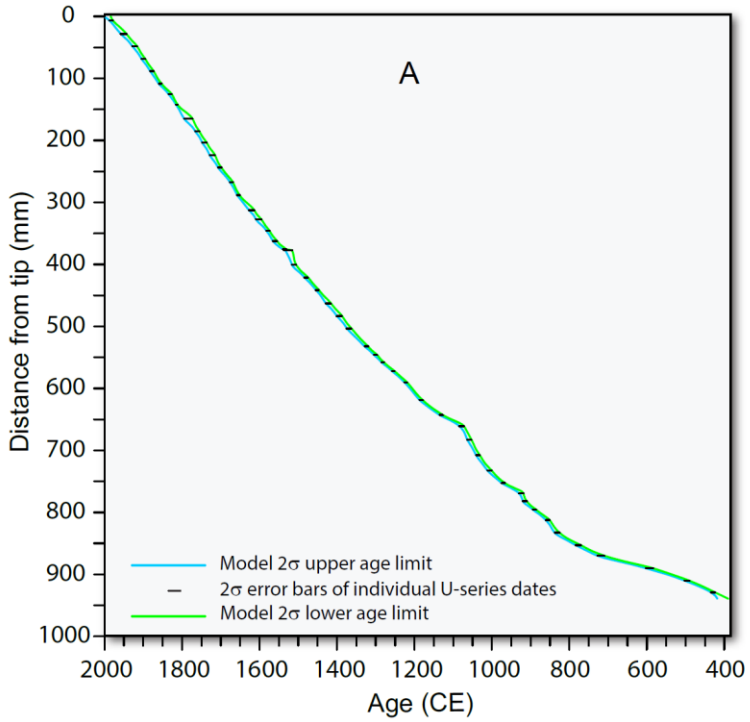

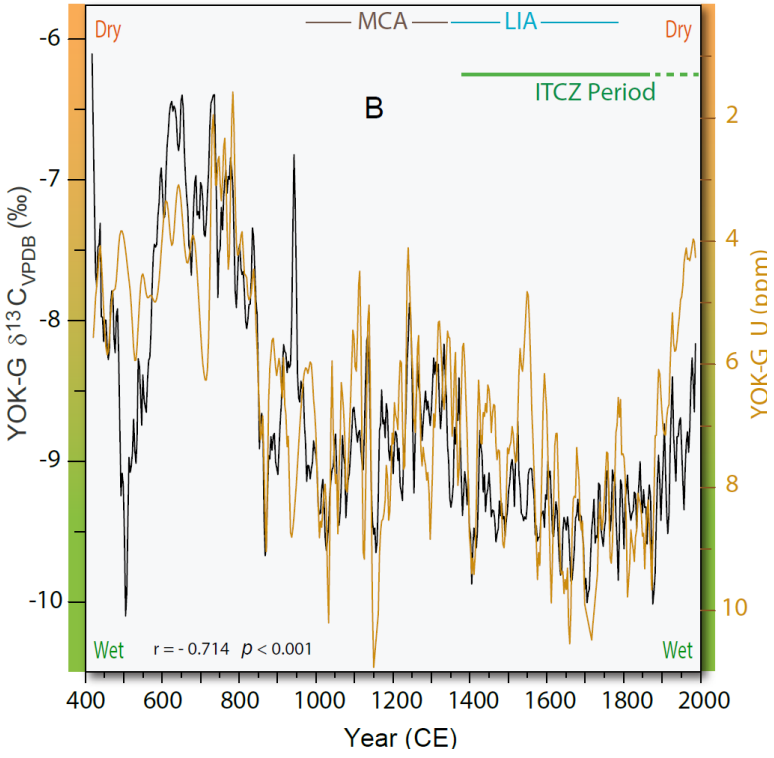

Figure 2. A. U-series-based age model for speleothem YOK-G. The model was constructed using the COPRA algorithm (14), and the 2σ uncertainty limits are shown as green (upper) and blue (lower) curves. Individual sample ages (52 ages) and their errors are denoted as black bars. B. $\delta^{13}C$ and U concentration data for YOK-G. Note the inverted axis for U concentrations (brown line) compared with $\delta^{13}C$ (black line).

Similarly, the $\delta^{18}O$ annual signal is less clear than the $\delta^{13}C$ annual signal, consistent with previous interpretations of YOK-G $\delta^{18}O$ as reflecting both rainfall amount and the rainfall $\delta^{18}O$, which is linked to tropical cyclones (*11*).

The highly resolved YOK-G $\delta^{13}C$ record enables the detection of seasonal- to millennial-scale climate variability (Fig. 2B). The early part of the record, ca. 400 – 900 CE is characterized by large shifts in

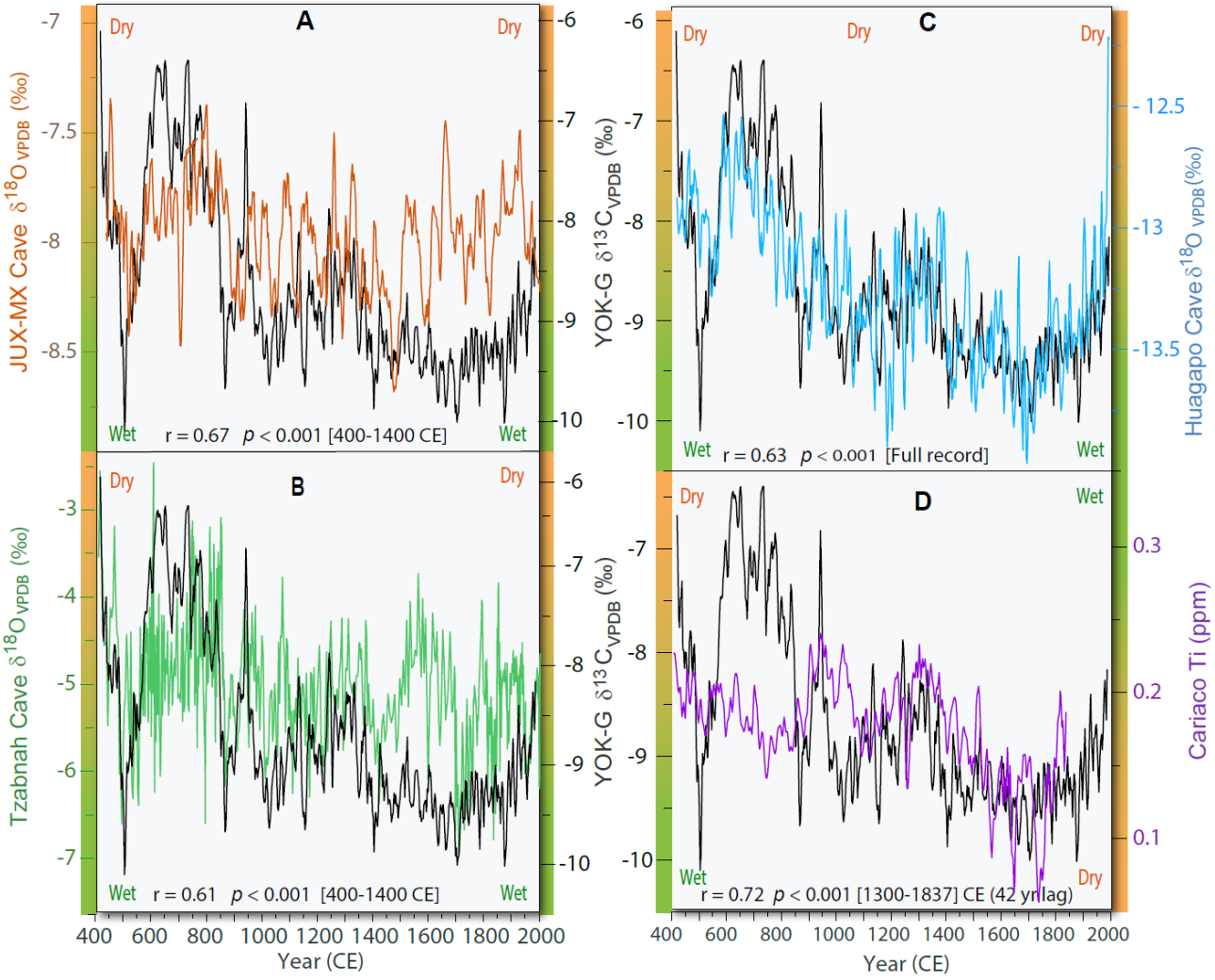

Figure 3. Comparison between YOK-G $\delta^{13}C$ and other rainfall proxy records at the northern and southern extent of the ITCZ. From north to south (A-C): A. The Juxtlahuaca Cave (stalagmite JUX-MX) $\delta^{18}O$ time-series (light brown) from SW Mexico (15), B. The Tzabnah Cave (Chaac stalagmite) $\delta^{18}O$ time-series (green line) from the northern Yucatan, Mexico (16), C. The Huagapo Cave $\delta^{18}O$ time-series (blue line) from the central Peruvian Andes (19). D. The Cariaco Basin Ti concentration record (purple)(4) Note that the Cariaco Ti axis is showing the opposite moisture trend (wet top). The best match for the full record is achieved between the two regions (Fig. 3C) that are located at the northern and southern margins of the ITCZ. Correlation statistics in each panel are for the time intervals indicated.

hydroclimate, including the most arid interval between 625-825 CE. A somewhat more humid climate was present from 900 - 1400 CE, during the Medieval Climate Anomaly (MCA), followed by an extended wet interval during the LIA and finally by progressive drying since the late 1800s CE (Fig. 1B). The

transition to the wettest interval from ~1400 CE to the late-1800s corresponds with a departure from the strong coherent variability with sites north of our study area, such as the annual-scale $\delta^{18}O$ moisture proxy (*15*) from Juxtlahuaca Cave ("JUX Cave") (Fig. 3B) in southwestern Mexico (17.44°N, 99.16°W) (Fig. 1). The JUX-MX record and YOK-G $\delta^{13}C$ data show coherent variability prior to 1400 CE ($r = 0.67$, $p < 0.001$) (Fig. 3A). In contrast, after the initiation of the LIA at ~1400 CE the two records diverge dramatically. The LIA in southwestern Mexico (Fig. 3A, B) is characterized by increased aridity, whereas in the YOK-G record this interval is characterized by high rainfall. Similarly, prior to 1400 CE a very good correlation ($r = 0.61$, $p < 0.001$) exists between YOK-G $\delta^{13}C$ and the Chaac stalagmite from Tzabnah Cave (20.73° N, 89.47° W) located near the Yucatan Peninsula's northwestern tip, north of Belize (*16*) (Figs 1 and 3B), a region currently receiving ~75% less annual rainfall than southern Belize (*17*) with little ITCZ influence.

We also compare the YOK-G data to records from the Southern Hemisphere ITCZ domain (Fig. 3B) represented by Huagapo Cave and the Cariaco Basin rainfall proxy datasets (Fig. 3C). The Huagapo Cave speleothem record (stalagmites P00-H1 & P09-H2) (*18*) from the central Peruvian Andes is one of the best-dated high-resolution records of South American monsoon dynamics. The large variability observed in the record was previously partially attributed to latitudinal shifts in Atlantic ITCZ position (*19*). A significant positive correlation ($r = 0.63$, $p < 0.001$) exists between the YOK-G $\delta^{13}C$ and the Huagapo Cave $\delta^{18}O$ record throughout the Common Era (Fig. 3C). This is remarkable given their large separation across the equator (Fig. 1). The peak LIA increase in South American monsoon strength implied by the Haugapo Cave record has been observed elsewhere, such as in the paired microalgal and mangrove biomarker $^{2}H/^{1}H$ record from the Galápagos (*6*) (Fig. 1), which was attributed to a southward shift of the ITCZ (*6*). Similarly, variability in the Cariaco Basin sediment titanium (Ti) concentration was previously attributed to changes in hydroclimate of the onshore watershed that drains into the basin, driven by meridional shifts in ITCZ position (*4*), where high Ti concentrations correspond to wetter than normal climate and low Ti concentrations to drier than normal climate conditions. The Cariaco Ti concentration data are strongly correlated with the YOK-G $\delta^{13}C$ data ($r = 0.72$, $p < 0.001$, 42 year lag) (Fig. 3D) after ~1300 CE. The lead-lag issue is likely related to the larger age errors of the untuned Ti time-series. The drying trend during the LIA in the Cariaco Basin watershed was attributed to southward migration of the ITCZ (*4*). It is not possible to reconcile these very high-quality hydroclimate records from both sides of the equator by invoking meridional ITCZ shifts exclusively. If the LIA was characterized by a simple southward ITCZ shift, it should have led to drying in our study area, which is contrary to the observed shift to much wetter conditions. Our data, considered on their own, would suggest a northward shift of the ITCZ. All the seemingly contradictory cross-equatorial datasets are reconciled by invoking an alternative model whereby the ITCZ expands meridionally but weakens in the central equatorial core region during globally cold climates, and contracts meridionally but strengthens in the core region during warm climates. This explanation is supported by recent modelling results (*7*) and modern rainfall data that reveal a narrowing of the Pacific ITCZ under modern warming (*20*).

A wavelet power spectra (*21, 22*) analysis of our YOK-G $\delta^{13}C$ data resampled at a constant 0.25 year resolution (Fig. 4A) illustrates that the pre-1400 CE portion of the spectra is characterized by weak multi-decadal variability but exhibits no annual-scale signal, whereas the post-1400 CE data show significant (95% confidence outlined in black) annual-scale variability, consistent with the dominant role of the modern annual ITCZ cycle. Broadly, we refer to the time after 1400 CE as the "ITCZ period", during

which the seasonal ITCZ excursion dominates hydroclimate at our site. Although ENSO exerts a strong influence on tropical hydroclimate, our wavelet analysis result (Fig. 4A) does not show ENSO type (interannual) periodicities, especially during

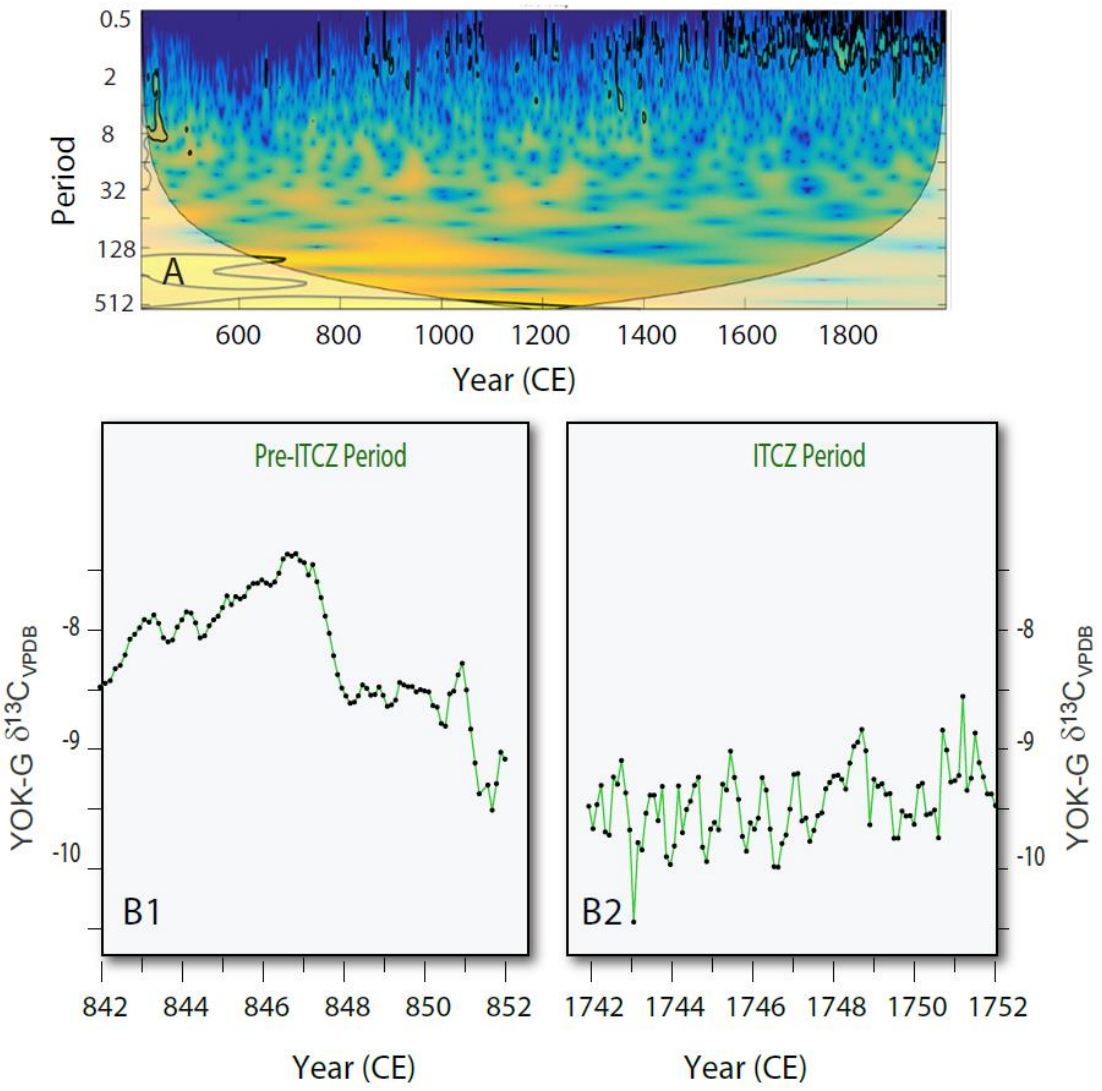

Figure 4. Wavelet spectral analysis of high-resolution YOK-G $\delta^{13}C$ data and detailed look at seasonal rainfall variability. A. Wavelet spectral output of the high resolution (0.25 year resolution) YOK-G $\delta^{13}C$ data. B. Difference in rainfall variability between the pre-ITCZ period and ITCZ period. Both segments were samples at the same, ~1.3 month, temporal resolution (small filled circles).

the ITCZ period. This observation is supported by modern rainfall data; there is no statistically significant correlation between ENSO and rainfall in our study area (Fig. S7). Our monthly scale $\delta^{13}C$ rainfall proxy data permit the reconstruction of paleoseasonality. We compare two decadal intervals, one from the

pre-ITCZ period (842-852 CE) (Fig. 4-B1) and another from the ITCZ period (1742-1842 CE) (Fig. 4-B2) sampled at about 1.3 month resolution. The pre-ITCZ period data (Fig. 4-B1) do not contain annual $\delta^{13}C$ cycles while the ITCZ period data (Fig. 4-B2) contains a well-developed annual signal. Strong seasonal rainfall cycles are expected in a regime dominated by the annual ITCZ cycle, as is currently the case. In contrast, the large inter-annual changes and very muted (or entirely absent) seasonal changes before 1400 CE suggest that the ITCZ did not reach the site of Yok Balum Cave prior ca. 1400 CE.

The contraction and expansion of the ITCZ does not preclude relative hemispherical shifts (the mean position of the ITCZ) in response to differential hemispherical warming and cooling as we showed previously in response to aerosol injections (*12*). Both modeling and hemispherical-scale rainfall data from both hemispheres support a meridional shift in the ITCZ clearly starting in the mid-20th Century (*23, 24*). But this effect is small compared to the pronounced drying at both peripheries of the tropics (Fig. 3) in response to the rapid warming in both hemispheres starting in the late-1800s (*25*).

A salient feature of our high-resolution data is that the Central America region is rapidly emerging from what we have called the ITCZ period that began in ~1400 CE (Fig. 2B). The bi-hemispherical relationships discussed here suggest that additional future warming is likely to lead to very dry conditions, last seen around 600-800 CE (Fig. 3). Our results imply that the ITCZ is not an intrinsic part of the Central American climate system but is instead a transient feature which most recently began affecting the region in ~1400 CE and whose influence has gradually waned since the mid-1800s. It is conceivable that the observed modern rainfall decrease could be the precursor to the ITCZ's complete abandonment of Central America in the future. Central American countries currently within the ITCZ's northern margin are experiencing growing food insecurity driven partially by climate change (*26*), leading to social upheaval and mass migration (*27*).

MATERIALS AND METHODS

Uranium-series methods. The ^{234}U-^{230}Th (uranium-series) chronology was performed at the Radiogenic Isotope Laboratory, the University of New Mexico. U-Th separation chemistry is described in Asmerom et al. (*28*). Part of this method was described by Ridley et al. (*12*) for the top 456 years. Because YOK-G is composed of aragonite, it has high uranium concentration (6.5 ppm on average) and thus we were able to use small samples, between 20-120 mg for obtaining a precise and accurate uranium-series age control per distance in stalagmite YOK-G. An aliquot of ^{233}U -^{236}U -^{229}Th high purity mixed spiked was added to each sample. U and Th were separated using 200-400 mesh chloride form anion exchange resin. U and Th isotopes were measured on a Thermo Neptune multi-collector inductively coupled plasma mass spectrometer (MC-ICP-MS). ^{233}U and ^{236}U and ^{232}Th were measured on Faraday cups with 10^{12} Ω resistors, while ^{235}U and ^{238}U were also measured on Faraday cups with 10^{11} Ω and 10^{10} Ω resistors, respectively. ^{234}U and ^{230}Th were measured on secondary electron multiplier (SEM) that sits behind a high-abundance filter. All measurements were done on static mode. Standards NBL-112 and an in-house ^{230}Th-^{229}Th solution were analyzed several times during the run sessions to accurately establish the gain between the SEM and Faraday cups. Initial ^{230}Th /^{232}Th ratio was estimated from the analysis of drip water and two carbonate powders obtained from the top of YOK-G during 2004 and 2006. We were able to derive an empirical relationship between $^{230}Th/^{232}Th$ atomic ratio, such that $^{230}Th/^{232}Th_{\text{atomic ratio (ppm)}} = 322.67*{}^{232}Th_{ppb}-0.269$. Half-life values from(*29*) were used for calculation of

the dates (Table S1). The accuracy and precision of the uranium-series ages were validated by Ridley et al. (*12*) for the top 456 years using the ^{14}C bomb signal and annual counting of $\delta^{13}C$ seasonal oscillations; the seasonal $\delta^{13}C$ cycles were used as the main chronology for that publication. For the longer record discussed here we constructed a robust age model using the computer algorithm COPRA (*14*). The COPRA model ages and the annually-resolved ages agree within the age uncertainties of the model ages. We have used the U-Th chronology for the entirety of the record here, including the top 456 years, to provide a continuity of method, but the U-Th chronology is extremely similar to the seasonal $\delta^{13}C$ cycle counting chronology, although the latter is probably somewhat more precise and was used in previous publications regarding YOK-G (*11, 12*).

Uranium concentration data. Uranium concentration data were obtained at the Radiogenic Isotope Laboratory at the University of New Mexico. Samples, between 3-10 mg, were dissolved in 3% nitric acid, diluted and spiked with ^{115}In. The samples and standards were analyzed using a Thermo X-series II inductively coupled plasma mass spectrometer (ICP-MS). Analytical precision (2σ) ranged between 0.2 to 6 % depending on concentration.

Stable isotope analysis. A total of 7,151 stable isotope analyses were measured along the growth axis of YOK-G covering a period between 2006 and 404 C.E., with an average resolution of 0.22 years, but with higher than monthly resolution across certain intervals. In order to get this unprecedented resolution, YOK-G was continuously milled at 0.1 mm across most of the sample and at 0.2 mm across some intervals. Stable isotope analysis for the first 456 years was reported on in Ridley et al. (*12*) , and here we discuss the record back to 404 C.E.. The majority of stable isotope analyses were conducted at Durham University using a Thermo MAT 253 Isotope-Ratio Mass Spectrometer with a Gasbench II (external precision of about 0.05- 0.10‰) on-line gas preparation and introduction system. Each sample 220-250 μg in size was reacted with 10 drops of orthophosphoric acid (H_3PO_4) under a helium (grade 5) atmosphere. The solution was left to digest at 50 °C for two hours. In addition, 14 external and in-house standards were run with each batch (50) of samples. In total, 5,644 stable isotope samples were run at Durham, and the others were obtained at Yale University (1,132 samples) and the University of New Mexico (375 samples) following similar procedures as at Durham. Interlab comparisons were facilitated using replicate samples, alternating samples, and standards. Additional comparison analyses were done on a Kiel IV automated carbonate preparation device via phosphoric acid digestion connected to a Thermo Delta V Plus mass spectrometer at the Las Vegas Isotope Science Laboratory at the University of Nevada, Las Vegas. The replicate $\delta^{13}C$ results agreed within their respective internal precisions (see Fig. S3).

Growth rate inference. In addition to the isotopic and elemental proxies, stalagmite growth rate can be an indicator of hydroclimate (*12, 30*), although the response depends on the moisture regime. In moisture-limited regimes growth thickness often correlates positively with rainfall amount (*30, 31*), whereas in very humid regimes the correlation can be inverse (*32*). Consequently, the growth rate response to rainfall can vary considerably on short time-scales, depending on drip water ionic strength changes. We were able to infer rough growth rate using the distances between the model age points obtained using COPRA (*14*) shown in Fig. S6. In the case of YOK-G, significant negative correlations exists between $\delta^{13}C$ and growth thickness ($r = -0.64$, $p < 0.001$) (Fig. S6), suggesting that more rainfall produces thicker laminae. Remarkable correlations between our $\delta^{13}C$ time-series and other regional and global climate proxies discussed here provide additional strong support for their use as hydroclimate proxies.

Age model. A robust age model with fully propagated errors was constructed using the program COPRA (*14*) that utilizes a Monte Carlo simulation and a translation procedure that allows for calculation of proxy time-series age uncertainties from radiometric date uncertainties. Annual geochemical layer counting of the top 365 mm (1550-1983 C.E.) shows excellent agreement with the uranium-series ages (*12*). Although the chronology used for the earlier shorter studies (*11-13*) was based on the geochemical layer count, here we utilize exclusively a uranium-series chronology in order to maintain the same dating technique throughout the entire extended record.

Data treatment and statistics. Smoothing, interpolation and correlation were done in Matlab. The YOK-G $\delta^{13}C$ data have a mean resolution of 0.22 years, whereas the uranium concentration data has a mean resolution of ~3 years. A number of other records have different resolutions. For the correlation work, the data were interpolated to the lower resolutions of two records. The significance of the r values were determined first by getting a new effective degree of freedom (EDOF) for each data set using the method of Bretherton et al. (*33*), as follows:

$$\mathrm{EDOF} = \mathrm{N}\,\frac{(1-r_1 r_{2)}}{(1+r_{1r_2})} \qquad (1)$$

Where, **N** is the length of the time series and r_1 and r_2, the lag-one autocorrelation. Using the new reduced degree of freedom, a set of t values were calculated. The *p*-value for each correlation coefficient shown is less than the stated threshold value for two-tailed t values. Thus a *p* value between 0.005 and 0.001 is shown as $p < 0.005$. The values that are lower than 0.001, regardless of how low, are simply shown as $p < 0.001$.

Unlike YOK-G and JUX-MX, the Tzabnah Cave (Chaac), northern Yucatan, Mexico (*16*) is composed of low-uranium calcite and consequently the ages have large errors associated with uncertainties in the initial $^{230}Th/^{232}Th$ ratios. The ages for Tzabnah Cave were tuned, within the age uncertainties, using the accurate and precise YOK-G age model. The uranium-series ages for the three speleothems compared in Fig. 3A and 3B (YOK-G, JUX-MX and Tzabnah Cave) were done in the first author's lab. The data were tuned within the age uncertainties using the accurate and precise YOK-G age model (shown in Fig. 3b).

Wavelet analysis was done using a Matlab program by Grinsted et al., (*21*) following the initial formulation by Torrence and Compo (*22*).

SUPPLEMENTARY MATERIALS

Supplementary material for this article is available at

Fig. S1. Location Map of the study site, Yok Balum Cave, southern Belize.

Fig. S2. Temperature and relative humidity data.

Fig. S3. Results from duplicate analyses using Kiel and Gasbench inlet systems.

Fig. S4. YOK-G $\delta^{13}C$ vs rainy season (June – October) rainfall data.

Fig. S5. YOK-G $\delta^{13}C$ vs growth rate.

Fig. S6. YOK-G $\delta^{18}O$ and U concentration data.

Fig. S7. Annual Oceanic Nino Index (ONI) vs rainy season monthly averages rainfall data.

Table S1. Uranium-series chronology data

REFRENCES AND NOTES:

1. Core_Writing_Team. (IPCC Geneva, Switzerland, 2014), pp. 151.
2. R. Neukom *et al.*, Inter-hemispheric temperature variability over the past millennium. *Nature Climate Change* **4**, 362 (2014).
3. F. M. Chambers, S. A. Brain, D. Mauquoy, J. McCarroll, T. Daley, The 'Little Ice Age'in the Southern Hemisphere in the context of the last 3000 years: Peat-based proxy-climate data from Tierra del Fuego. *The Holocene* **24**, 1649-1656 (2014).
4. G. H. Haug, K. A. Hughen, D. M. Sigman, L. C. Peterson, U. Röhl, Southward migration of the intertropical convergence zone through the Holocene. *Science* **293**, 1304-1308 (2001).
5. F. A. Lechleitner *et al.*, Tropical rainfall over the last two millennia: evidence for a low-latitude hydrologic seesaw. *Scientific Reports* **7**, 45809 (2017).
6. D. B. Nelson, J. P. Sachs, Galápagos hydroclimate of the Common Era from paired microalgal and mangrove biomarker 2H/1H values. *Proceedings of the National Academy of Sciences* **113**, 3476-3481 (2016).
7. M. P. Byrne, T. Schneider, Narrowing of the ITCZ in a warming climate: Physical mechanisms. *Geophysical Research Letters* **43**, (2016).
8. N. Scroxton *et al.*, Hemispherically in-phase precipitation variability over the last 1700 years in a Madagascar speleothem record. *Quaternary Science Reviews* **164**, 25-36 (2017).
9. R. F. Denniston *et al.*, Expansion and contraction of the Indo-Pacific tropical rain belt over the last three millennia. *Scientific Reports* **6**, 34485 (2016).
10. G. Poveda, P. R. Waylen, R. S. Pulwarty, Annual and inter-annual variability of the present climate in northern South America and southern Mesoamerica. *Palaeogeography, Palaeoclimatology, Palaeoecology* **234**, 3-27 (2006).

11. L. M. Baldini *et al.*, Persistent northward North Atlantic tropical cyclone track migration over the past five centuries. *Scientific reports* **6**, 37522 (2016).
12. H. E. Ridley *et al.*, Aerosol forcing of the position of the intertropical convergence zone since AD 1550. *Nature Geoscience* **8**, 195-200 (2015).
13. R. A. Jamieson *et al.*, Intra-and inter-annual uranium concentration variability in a Belizean stalagmite controlled by prior aragonite precipitation: A new tool for reconstructing hydro-climate using aragonitic speleothems. *Geochimica et Cosmochimica Acta* **190**, 332-346 (2016).
14. S. F. Breitenbach *et al.*, Constructing proxy records from age models (COPRA). *Climate of the Past* **8**, 1765-1779 (2012).
15. M. S. Lachniet, Y. Asmerom, V. Polyak, J. P. Bernal, Two millennia of Mesoamerican monsoon variability driven by Pacific and Atlantic synergistic forcing. *Quaternary Science Reviews* **155**, 100-113 (2017).
16. M. Medina-Elizalde *et al.*, High resolution stalagmite climate record from the Yucatán Peninsula spanning the Maya terminal classic period. *Earth and Planetary Science Letters* **298**, 255-262 (2010).
17. P. M. Douglas *et al.*, Drought, agricultural adaptation, and sociopolitical collapse in the Maya Lowlands. *Proceedings of the National Academy of Sciences*, 201419133 (2015).
18. L. C. Kanner, S. J. Burns, H. Cheng, R. L. Edwards, M. Vuille, High-resolution variability of the South American summer monsoon over the last seven millennia: insights from a speleothem record from the central Peruvian Andes. *Quaternary Science Reviews* **75**, 1-10 (2013).
19. M. Vuille *et al.*, A review of the South American monsoon history as recorded in stable isotopic proxies over the past two millennia. *Climate of the Past* **8**, 1309-1321 (2012).
20. K. Wodzicki, A. Rapp, Long‐term characterization of the Pacific ITCZ using TRMM, GPCP, and ERA‐Interim. *Journal of Geophysical Research: Atmospheres* **121**, 3153-3170 (2016).
21. A. Grinsted, J. C. Moore, S. Jevrejeva, Application of the cross wavelet transform and wavelet coherence to geophysical time series. *Nonlinear processes in geophysics* **11**, 561-566 (2004).
22. C. Torrence, G. P. Compo, A practical guide to wavelet analysis. *Bulletin of the American Meteorological society* **79**, 61-78 (1998).
23. Y. T. Hwang, D. M. Frierson, S. M. Kang, Anthropogenic sulfate aerosol and the southward shift of tropical precipitation in the late 20th century. *Geophysical Research Letters* **40**, 2845-2850 (2013).
24. X. Zhang *et al.*, Detection of human influence on twentieth-century precipitation trends. *Nature* **448**, 461 (2007).
25. J. Hansen, R. Ruedy, M. Sato, K. Lo, Global surface temperature change. *Reviews of Geophysics* **48**, (2010).
26. C. A. Harvey *et al.*, Climate change impacts and adaptation among smallholder farmers in Central America. *Agriculture & Food Security* **7**, 57 (2018).
27. R. Reuveny, Climate change-induced migration and violent conflict. *Political geography* **26**, 656-673 (2007).
28. Y. Asmerom, V. J. Polyak, S. J. Burns, Variable winter moisture in the southwestern United States linked to rapid glacial climate shifts. *Nature Geoscience* **3**, 114 (2010).
29. H. Cheng *et al.*, Improvements in 230Th dating, 230Th and 234U half-life values, and U–Th isotopic measurements by multi-collector inductively coupled plasma mass spectrometry. *Earth and Planetary Science Letters* **371**, 82-91 (2013).
30. Y. Asmerom, V. J. Polyak, J. B. Rasmussen, S. J. Burns, M. Lachniet, Multidecadal to multicentury scale collapses of Northern Hemisphere monsoons over the past millennium. *Proceedings of the National Academy of Sciences* **110**, 9651-9656 (2013).

411 31. V. J. Polyak, Y. Asmerom, Late Holocene climate and cultural changes in the southwestern
412 United States. *Science* **294**, 148-151 (2001).
413 32. C. Proctor, A. Baker, W. Barnes, M. Gilmour, A thousand year speleothem proxy record of North
414 Atlantic climate from Scotland. *Climate Dynamics* **16**, 815-820 (2000).
415 33. C. S. Bretherton, M. Widmann, V. P. Dymnikov, J. M. Wallace, I. Bladé, The effective number of
416 spatial degrees of freedom of a time-varying field. *Journal of climate* **12**, 1990-2009 (1999).

417 **Acknowledgements:** We thank the Belize Institute of Archeology for research permit (2006-2008) to
418 KMP and access to the Cave by the land owner, Santa Cruz Village, UKAA. This research was supported
419 by grants from the National Science Foundation: NSF-BCS 0620445 (KMP), NSF-HSD 0827305 (KMP &
420 YA), NSF-EAR-0326902 (YA), NSF-HSD 0827312 (DJK et al.), and from the Alphawood Foundation (2009-
421 2014 to KMP), and the European Research Council (ERC240167 to JULB). Meteorological records
422 provided courtesy of HYDROMET, Government of Belize. **Author Contributions:** YA wrote the draft, VJP,
423 YA and VVA were responsible for uranium-series chronology, YA and VP for the trace element work and
424 JULB, HER, and CGM for stable isotope analysis. YA did the statistical and spectral analysis. DJK, KMP, YA
425 and SFMB conceived the original project. KMP, SFMB, JULB and HER were responsible for field work and
426 logistics. All authors contributed to refining the manuscript. **Competing interests:** The authors declare
427 that they have no competing interest. **Data and materials availability:** All data needed to evaluate the
428 conclusions in the paper are present in the paper and/or the Supplementary Materials. Additional data
429 related to this paper may be requested from the authors.

Supplementary Materials for:

Intertropical Convergence Zone Variability in the Neotropics During the Common Era

Yemane Asmerom*, James U. L. Baldini, Keith M. Prufer, Victor Polyak, Harriet E. Ridley, Valorie V. Aquino, Lisa M. Baldini, Sebastian F. M. Breitenbach, Colin G. Macpherson, & Douglas J. Kennett

*Corresponding author: asmerom@unm.edu

The PDF file includes:

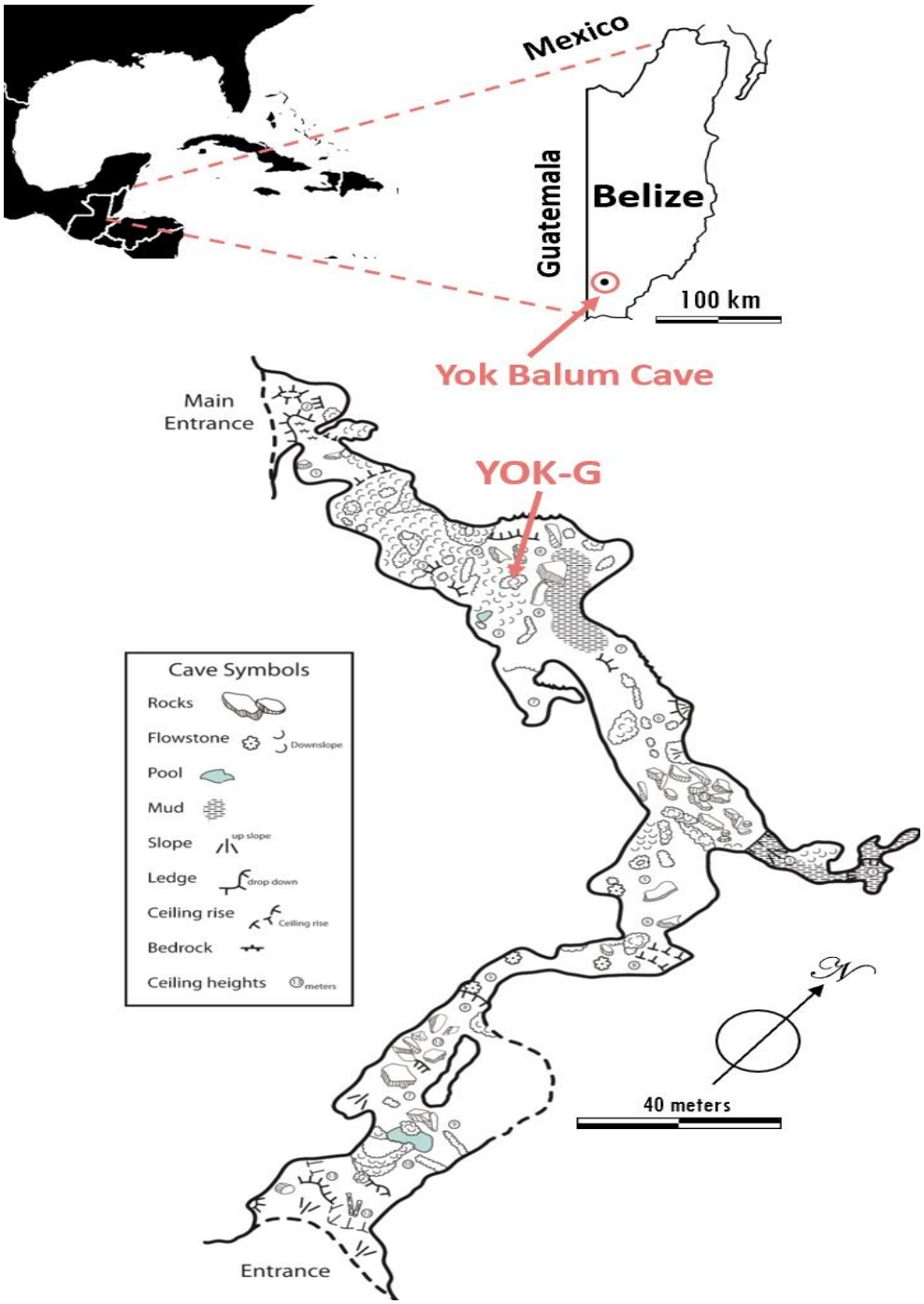

Fig. S1. Location Map. Yok Balum Cave is located in southern Belize [160 12' 30.780" N, 890 4' 24.420" W] at an elevation of 336 meters above sea level. The cave has perennial pools of water and is at 100% humidity (Fig. S2). Figure is adapted from the tape, compass, and clinometer map of the cave produced by Thomas Miller for the project.

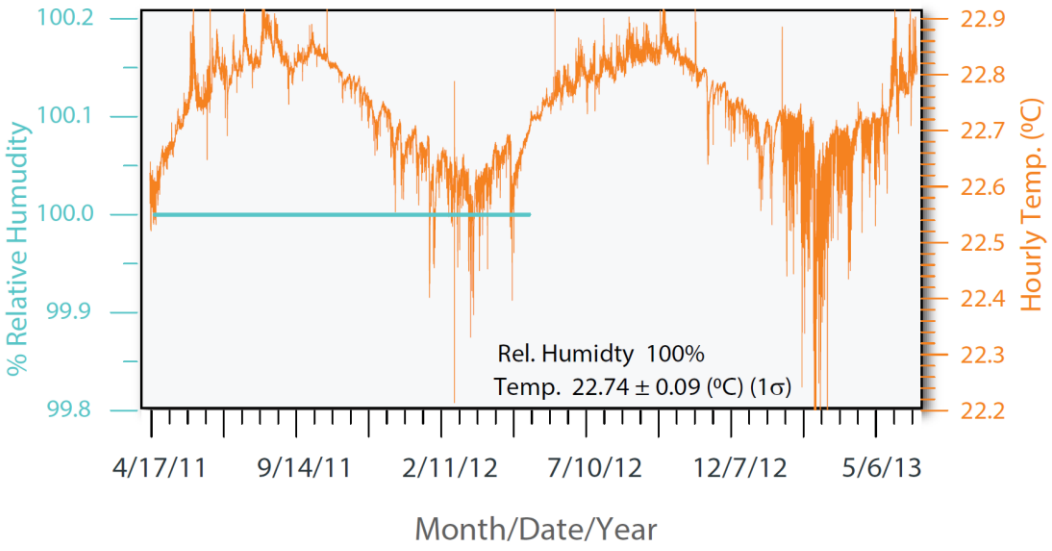

Fig. S2. Temperature and relative humidity data. Results of over two years hourly temperature data shown on an expanded scale. The temperature was 22.74 ± 0.09 (^{0}C) (1σ) over the time of monitoring (between April 2011 and May 2013). The relative humidity was monitored for a little over a year and was always at 100% (12).

Fig. S3. Results from duplicate analyses using Kiel and Gasbench inlet systems. The results are within the 2σ uncertainties of both analyses (~ 0.1 ‰).

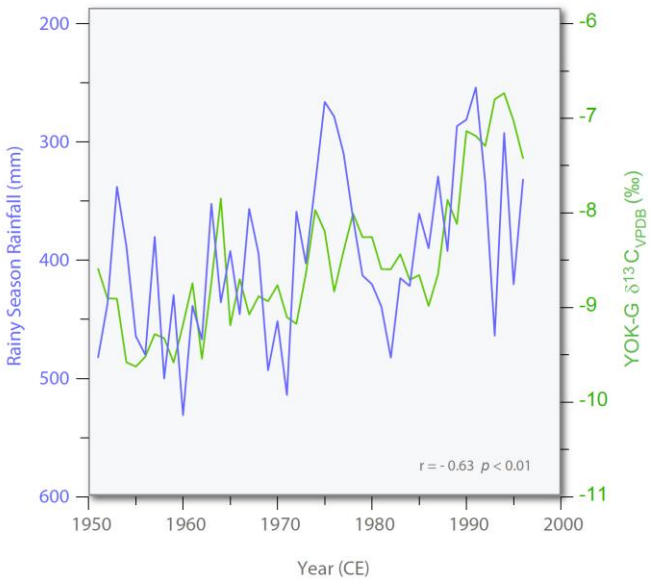

Fig. S4. $\delta^{13}C$ vs rainy season (June – October) rainfall data. The graph is based on the average multi-station rain gauge data from stations located within a radius of 125 km of our study area. The $\delta^{13}C$ data capture the short time variability and the overall drying trend.

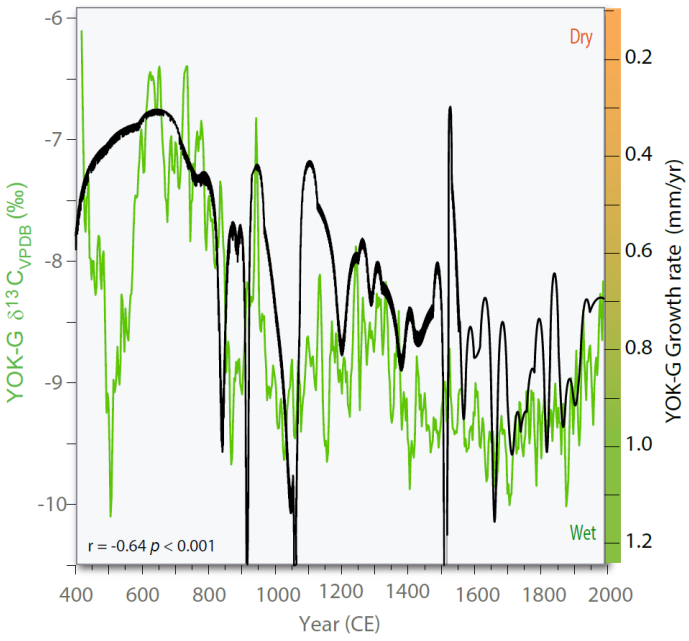

Fig. S5. Comparison between isotope data and growth rate. YOK-G growth rate versus a) $\delta^{13}C$ ($r = -0.64$, $p < 0.001$) Note: growth rate is measured using U-series age distances. In this case, the growth rate captures the large shifts in the $\delta^{13}C$ data. The relationship between growth rate and amount of precipitation is not always direct, however.

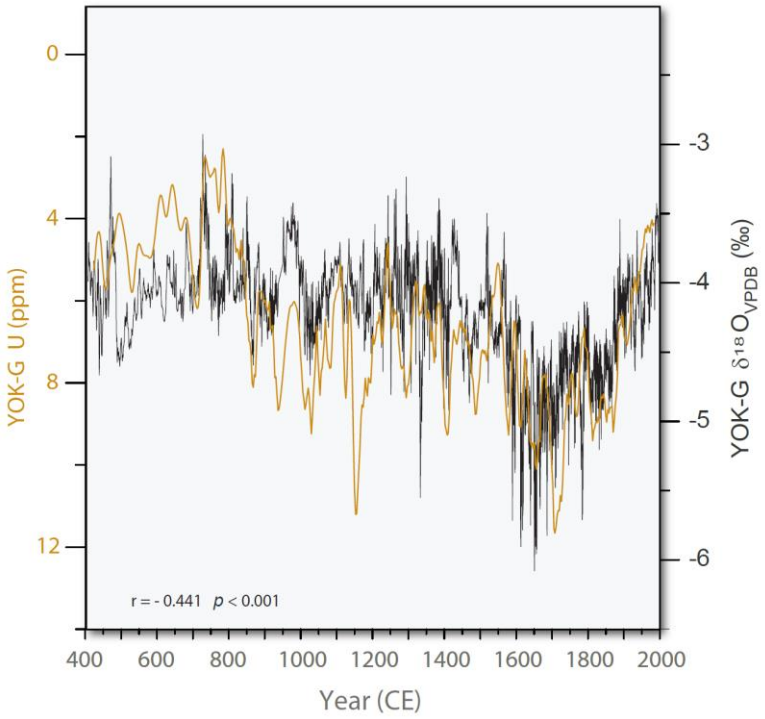

Fig. S6. $\delta^{18}O$ and U concentration data for YOK-G. Note the flipped axis for uranium concentrations (orange line) compared with $\delta^{18}O$ (black line) r = -0.44, $p < 0.001$. The match between the two proxies is not as good as that for U concentration and $\delta^{13}C$ (r= -0.71, $p < 0.001$). The $\delta^{18}O$ data capture a variety of atmospheric processes (e.g. cyclones (11) in addition to local hydroclimate.

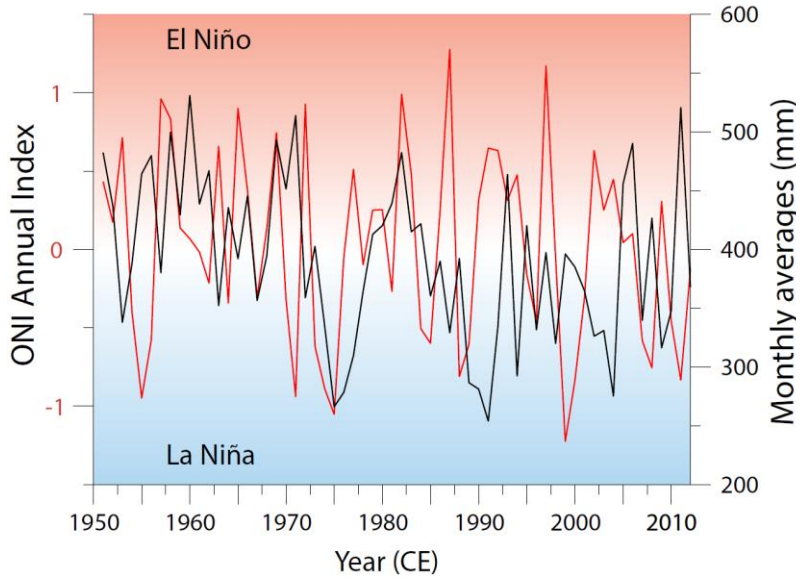

Fig. S7. Annual Oceanic Nino Index (ONI) vs rainy season monthly averages rainfall data. Although ENSO plays an important role in interannual rainfall variability in the tropics, it does not seem to have a significant role in our study area (no statistically significant correlation between the ONI index and rainfall). This seems to have been the case also during the ITCZ phase (the period since ca. 1400 CE when the ITCZ annual cycle seems to be the dominant controller of annual rainfall). The wavelet analysis (Fig. 4A main text) supports this inference. Source of ONI data: https://www.esrl.noaa.gov/psd/data/correlation/oni.data

Table S1. Uranium-series chronology data

Depth (mm)	^{238}U (ng/g)	unc. 2σ	^{232}U (pg/g)	error 2σ	(^{230}Th/^{232}Th) activity	unc. 2σ	(^{230}Th/^{238}U) activity	unc. 2σ	δ^{234}U‰ Measured	unc. 2σ	δ^{234}U‰ Initial	unc. 2σ	Age Uncorr	unc. 2σ	Age Corr.	unc. 2σ	Age (C.E.)	unc. 2σ
6.6	5200	± 5	270	± 57	32	± 7	0.00054	± 0.00003	467	± 1	467	± 1	40	± 2	23	± 5	1983	± 5
28.3	4497	± 9	86	± 73	136	± 116	0.00086	± 0.00004	467	± 1	467	± 1	64	± 3	55	± 8	1951	± 8
48.0	5154	± 5	58	± 60	331	± 345	0.00121	± 0.00003	483	± 1	483	± 1	89	± 2	84	± 6	1922	± 6
68.5	6644	± 7	27	± 50	1110	± 2057	0.00148	± 0.00002	488	± 1	488	± 1	109	± 1	106	± 5	1900	± 5
88.3	8352	± 7	7	± 42	6471	± 39632	0.00173	± 0.00001	464	± 1	464	± 1	129	± 1	128	± 4	1878	± 4
108.4	5784	± 5	59	± 39	631	± 422	0.00210	± 0.00002	485	± 1	485	± 1	154	± 2	150	± 4	1856	± 4
125.2	7773	± 4	31	± 50	1887	± 3099	0.00242	± 0.00003	489	± 1	489	± 1	178	± 2	175	± 4	1831	± 4
142.4	17083	± 20	117	± 60	1206	± 619	0.00270	± 0.00002	508	± 2	508	± 2	195	± 2	193	± 2	1813	± 2
165.0	6416	± 5	4	± 66	15952	± 281458	0.00304	± 0.00003	491	± 1	492	± 1	223	± 2	222	± 11	1784	± 11
185.3	6754	± 5	35	± 57	2017	± 3322	0.00338	± 0.00003	486	± 1	486	± 1	248	± 2	245	± 5	1761	± 5
203.4	7932	± 7	17	± 61	5051	± 17887	0.00359	± 0.00003	477	± 1	477	± 1	265	± 2	264	± 6	1742	± 6
223.6	8387	± 10	5	± 55	21475	± 258268	0.00385	± 0.00002	474	± 1	475	± 1	285	± 2	284	± 7	1722	± 7
243.9	10095	± 25	8	± 47	15310	± 86993	0.00413	± 0.00002	480	± 1	481	± 1	304	± 2	304	± 4	1702	± 4
267.3	8099	± 14	49	± 47	2287	± 2173	0.00457	± 0.00003	481	± 1	481	± 1	337	± 2	334	± 4	1672	± 4
288.3	8629	± 15	64	± 40	1982	± 1241	0.00479	± 0.00003	471	± 1	472	± 1	355	± 2	352	± 3	1654	± 3
312.5	5674	± 18	80	± 66	1130	± 937	0.00521	± 0.00006	451	± 2	451	± 2	392	± 4	386	± 7	1620	± 7
327.2	6238	± 10	14	± 53	7679	± 30144	0.00546	± 0.00005	471	± 1	471	± 1	405	± 4	404	± 7	1602	± 7
345.7	7440	± 11	106	± 56	1253	± 664	0.00583	± 0.00003	469	± 1	470	± 1	434	± 3	428	± 4	1578	± 4
362.5	4894	± 4	21	± 38	4219	± 7602	0.00601	± 0.00002	462	± 1	462	± 1	449	± 2	447	± 5	1559	± 5
375.5	6387	± 6	143	± 54	879	± 331	0.00645	± 0.00003	469	± 1	470	± 1	480	± 2	471	± 4	1535	± 4
377.3	3939	± 4	22	± 52	3530	± 8293	0.00654	± 0.00008	477	± 1	478	± 1	484	± 6	480	± 10	1526	± 10
400.5	4165	± 3	117	± 45	738	± 284	0.00681	± 0.00004	469	± 1	469	± 1	507	± 3	495	± 5	1511	± 5
421.1	6200	± 5	48	± 42	2764	± 2424	0.00702	± 0.00004	446	± 1	446	± 1	531	± 3	527	± 4	1479	± 4
441.6	6976	± 12	54	± 43	2977	± 2370	0.00754	± 0.00003	474	± 1	475	± 1	559	± 2	555	± 4	1451	± 4
463.1	4314	± 5	51	± 49	2041	± 1944	0.00789	± 0.00005	463	± 1	464	± 1	590	± 4	584	± 7	1422	± 7
483.4	4590	± 5	58	± 55	2043	± 1939	0.00844	± 0.00004	493	± 1	494	± 1	618	± 3	612	± 6	1394	± 6
503.4	4010	± 4	53	± 40	2026	± 1526	0.00880	± 0.00003	496	± 1	497	± 1	643	± 3	637	± 6	1369	± 6
532.2	6509	± 4	55	± 50	3358	± 3063	0.00935	± 0.00003	490	± 1	491	± 1	686	± 2	682	± 4	1324	± 4
546.1	5081	± 3	157	± 42	955	± 259	0.00963	± 0.00003	469	± 1	470	± 1	717	± 2	706	± 4	1300	± 4
557.7	8218	± 6	252	± 49	990	± 192	0.00993	± 0.00003	480	± 1	481	± 1	734	± 2	724	± 3	1282	± 3
572.0	9897	± 8	111	± 59	2763	± 1472	0.01010	± 0.00003	462	± 1	463	± 1	756	± 2	751	± 3	1255	± 3
590.2	8368	± 6	55	± 45	4933	± 4080	0.01054	± 0.00003	465	± 1	466	± 1	787	± 2	784	± 3	1222	± 3
618.7	6811	± 4	118	± 41	1996	± 871	0.01136	± 0.00003	497	± 1	498	± 1	830	± 3	823	± 4	1183	± 4
642.8	5473	± 4	55	± 52	1996	± 2716	0.01216	± 0.00003	512	± 2	513	± 2	880	± 3	875	± 4	1131	± 4
660.9	4715	± 3	123	± 56	1502	± 678	0.01285	± 0.00005	499	± 1	500	± 2	938	± 4	928	± 6	1078	± 6
682.8	6366	± 4	86	± 63	2937	± 2160	0.01304	± 0.00004	496	± 1	497	± 1	954	± 3	948	± 5	1058	± 5
707.5	11551	± 9	21	± 72	22320	± 75647	0.01336	± 0.00003	506	± 2	508	± 2	971	± 3	970	± 5	1036	± 5
732.4	6575	± 8	319	± 74	869	± 202	0.01378	± 0.00005	488	± 1	489	± 1	1014	± 4	1000	± 5	1006	± 5
752.6	7378	± 8	191	± 59	1704	± 531	0.01440	± 0.00004	509	± 2	511	± 2	1044	± 3	1035	± 4	971	± 4
769.3	3528	± 4	155	± 41	1042	± 273	0.01499	± 0.00005	496	± 1	498	± 1	1098	± 4	1081	± 6	925	± 6
782.0	3840	± 2	179	± 36	992	± 200	0.01516	± 0.00004	499	± 1	501	± 2	1107	± 3	1091	± 5	915	± 5
795.4	5768	± 4	73	± 39	3729	± 2003	0.01534	± 0.00004	498	± 1	500	± 2	1122	± 3	1116	± 4	890	± 4
812.5	6509	± 5	140	± 59	2079	± 872	0.01594	± 0.00004	507	± 2	508	± 2	1159	± 3	1150	± 5	856	± 5
832.8	5114	± 5	52	± 54	4879	± 5050	0.01637	± 0.00005	520	± 2	522	± 2	1179	± 4	1174	± 6	832	± 6
853.0	4994	± 5	107	± 64	2461	± 1483	0.01724	± 0.00005	526	± 2	528	± 2	1238	± 4	1229	± 7	777	± 7
869.8	2814	± 3	240	± 58	650	± 158	0.01811	± 0.00007	510	± 2	512	± 2	1315	± 5	1287	± 9	719	± 9
890.2	4229	± 5	29	± 60	8687	± 18201	0.01937	± 0.00006	499	± 1	501	± 2	1417	± 5	1413	± 9	593	± 9
910.1	5697	± 5	447	± 64	797	± 114	0.02045	± 0.00006	465	± 1	467	± 1	1532	± 5	1510	± 6	496	± 6
929.1	5694	± 4	187	± 48	1984	± 514	0.02132	± 0.00005	473	± 1	475	± 1	1589	± 4	1577	± 5	429	± 5

Unc. 2σ uncertainties, wt.avg=weighted avarage ages, δ^{234}U (‰) = ([234U/238U]activity – 1) x 1000. Decay constants from Cheng et al (29). See Materials and Methods section for initial ^{230}Th/^{232}Th correction procedure. All errors are 2σ (absolute).